

Distributed Video Adaptive Block Compressive Sensing

JOSEPH ZAMMIT¹, (Member, IEEE), IAN J. WASSELL¹. (Member, IET)

¹Computer Laboratory, William Gates Building, 15 JJ Thomson Ave, Cambridge CB3 0FD, United Kingdom

Corresponding author: Joseph Zammit (e-mail: jz390@cl.cam.ac.uk).

The authors would like to thank and acknowledge funding from the Cambridge Trust, the Engineering and Physical Sciences Research Council Centre for Doctoral Training in Sensor Technologies and Applications (EP/L015889/1), and the Endeavour (Malta) Scholarships Scheme.

arXiv:2104.00636v1 [eess.IV] 1 Apr 2021

ABSTRACT Video block compressive sensing has been studied for use in resource constrained scenarios, such as wireless sensor networks, but the approach still suffers from low performance and long reconstruction time. Inspired by classical distributed video coding, we design a lightweight encoder with computationally intensive operations, such as video frame interpolation, performed at the decoder. Straying from recent trends in training end-to-end neural networks, we propose two algorithms that leverage convolutional neural network components to reconstruct video with greatly reduced reconstruction time. At the encoder, we leverage temporal correlation between frames and deploy adaptive techniques based on compressive measurements from previous frames. At the decoder, we exploit temporal correlation by using video frame interpolation and temporal differential pulse code modulation. Simulations show that our two proposed algorithms, VAL-VFI and VAL-IDA-VFI reconstruct higher quality video, achieving state-of-the-art performance.

INDEX TERMS Distributed Video Compressive Sensing, Adaptive Block Compressive Sensing

I. INTRODUCTION

TRANSMITTING video continuously from resource constrained sensors is very challenging because of the need to capture, compress and transmit video as power efficiently as possible, video being one of the highest bit rate signals possible. Classical distributed video coding (DVC) techniques assume implicitly that capturing video is power-efficient, and focus on compressing video as efficiently as possible, so that it can be transmitted viably from the sensor. This means that computationally intensive operations, such as motion compensated prediction (MCP), have to be moved to the decoder. This would lead to a rise in transmission bitrate, and is countered by transmitting some of the frames at a lower bit rate, normally resulting in lower visual quality at the decoder. However, we can leverage the correlation between frames to restore video quality. The distributed source coding theories of Slepian and Wolf [1] and Wyner and Ziv [2], inform us that we can transmit correlated data without exploiting correlation at the encoder, at a lower rate than that required if we assume the data is uncorrelated, and still recover the full information at the decoder.

Compressive sensing (CS) [4], [5] represents a departure from the normal source coding paradigm, of sampling an analogue signal at the Nyquist rate, digitizing the samples at the

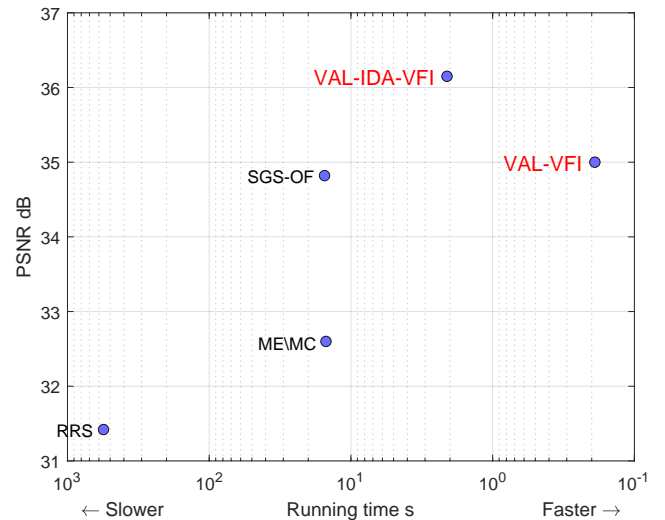


FIGURE 1. PSNR (dB) versus execution time per frame (s) for Video CS algorithms, calculated for the first 17 frames of six CIF video sequences described in section IV. SGS-OF [3] PSNR and execution time are reported from the original paper, that employed a comparable simulation platform.

highest possible signal-to-quantization-noise-ratio and then using complex source coding algorithms to compress the data

as much as possible. In CS, the capture and compress processes are combined to obviate the need for computationally-intensive source coding algorithms. However, using information theoretic arguments, Goyal [6] cautions that the compression factors achievable with CS alone, are lower than those that can be achieved by classical source coding paradigms. This means that some form of low-complexity source coding is still required prior to transmission.

CS senses a multidimensional signal $\mathbf{x} \in \mathbb{R}^N$ by performing the inner product between all the components of vector \mathbf{x} and rows of a measurement matrix $\Phi \in \mathbb{R}^{M \times N}$. The CS operation generates an M dimensional compressed signal $\mathbf{y} = \Phi \mathbf{x}$, that is $\mathbf{y} \in \mathbb{R}^M$. This reduces the dimensionality of \mathbf{x} from N to the dimensionality of \mathbf{y} , achieving a compression ratio, $\delta = M/N$. Note that a higher compression ratio means more measurements.

Applying CS to video frames requires the storage of the measurement matrix $\Phi \in \mathbb{R}^{M \times N}$ at the encoder. Contemporary video CS techniques operate on a video signal with a group of pictures (GOP) structure. The leading key frame in the GOP is coded with a higher quality than the remaining non-key frames. The key frame is typically coded with a compression ratio δ in the range 0.4 to 0.7 in the literature [7] [8] [3]. This means that even for modest resolution, common intermediate format (CIF) video, that is with $N = 352 \times 288$ pixels per frame, the storage requirement of the measurement matrix $N_s = \delta \cdot N^2$ is of the order of gigabytes when representing each matrix coefficient by an integer (e.g., 16 bits) and is impractical for resource constrained sensors. Generating the matrix on the fly would be too power inefficient. The solution to this problem, proposed in the literature [9], [10], is to break the video frames into sub-image blocks of size $B \times B$ pixels, where B is typically 4, 8, 16 or 32. The same measurement matrix is then used to compressively sense each block.

However, block-based CS of video frames comes with two problems. The first arises from the fact that the number of measurements M required by CS theory is proportional to the sparsity of the signal S , that is $M = kS \log(N/S)$, where k is a constant with typical values in the range $\{2 \dots 6\}$ [11]. The sparsity is the number of non-zero coefficients, in some domain Ψ , that can represent the signal with the desired quality. If the video frame is processed as one block, there is one sparsity value for the frame. With block-based processing, each block has its own sparsity level, that is changing from frame to frame. In adaptive block-based image CS, the sparsity of each block is estimated prior to compressively sensing it [12]. The challenge is to estimate the sparsity with as low a complexity and overhead as possible.

The second problem caused by block-based coding, is that of blocking artefacts appearing in the reconstructed image, if the CS reconstruction is also block-by-block. This can be solved by applying deblocking filters or by sensing the image block-by-block but reconstructing it as a whole, using a full-image sensing matrix that is composed of the block sensing matrices on its diagonal, that is $\Phi_I = \text{diag}(\Phi_B)$ [9].

In the following, bold capital letters represent matrices, bold lower case letters represent vectors, and normal case letters, scalar values. Consider a multidimensional signal $\mathbf{x} \in \mathbb{R}^N$ with a sparse representation $\mathbf{f} \in \mathbb{R}^N$ in some domain Ψ , that is $\mathbf{f} = \Psi \mathbf{x}$. Then the compressive samples of \mathbf{y} , produced by the measurement matrix Φ are given by $\mathbf{y} = \Phi \Psi \mathbf{x} + \mathbf{n}$ where \mathbf{n} is the measurement noise. The reconstruction of \mathbf{x} requires the solution of this equation. However, this is an ill-posed problem because the sensing matrix $\mathbf{A} := \Phi \Psi \in \mathbb{R}^{M \times N}$ and $M \ll N$. A tractable solution can be pursued by first casting the problem as a convex linear program:

$$\min_{\mathbf{x}} \|\mathbf{x}\|_1, \quad \text{s.t.} \quad \|\mathbf{A}\mathbf{x} - \mathbf{y}\|_2^2 < \epsilon \quad (1)$$

where ϵ is a measure of the noise level, and solving it using state-of-the-art LP solvers. This is nontrivial and time consuming, and a significant number of reconstruction techniques have been proposed to accelerate the solution, such as matching pursuit [13], Bayesian [14], approximate message passing (AMP) [15] and denoising AMP (D-AMP) [16].

Recently, convolutional neural networks (CNNs) have been applied to solve equation (1) [17], [18], [19], [12]. A number of authors have proposed CNNs that can reconstruct compressively sensed images in 10's to 100's of milliseconds, such as Reconnet [20], CS-Net [21], ISTA-Net and ISTA-Net+ [22], and SCSNet [23]. The reconstruction times of these CNNs allows CS video to be transmitted at tens of frames per second, but without exploiting temporal correlation between frames, generating large bit-rates.

Video CS techniques have been proposed that exploit temporal correlation by multihypothesis prediction, motion compensated prediction or optical flow at the decoder such as ME/MC [7], RRS [8], and SGS-OF [3]. Recently video CS (VCS) has been reconstructed using CNNs, for example VCSNet [24].

In this paper we present a real-time video compressive sensing framework that leverages plug-and-play CNNs to exploit temporal correlation between frames at the decoder, using video-frame interpolation (VFI). The DAIN [25] VFI CNN allows our VCS adaptive linear DCT VFI (VAL-VFI) algorithm, shown in figure 1, to achieve state-of-the-art PSNR and MS-SSIM [26] performance. The main contributions of this paper are as follows:

- In a departure from the current focus to design decoders that execute solely on the GPU, we design hybrid decoders that use the GPU to accelerate two computationally intensive components of our proposed algorithms, video frame interpolation and full image reconstruction.
- We propose a video CS framework using adaptive linear DCT measurements (VAL) that exploits temporal correlation at the encoder and the decoder. At the encoder, two algorithms, THI and MDD are proposed to leverage temporal correlation by adapting the block measurements based on the transform coefficients measured in previous frames.

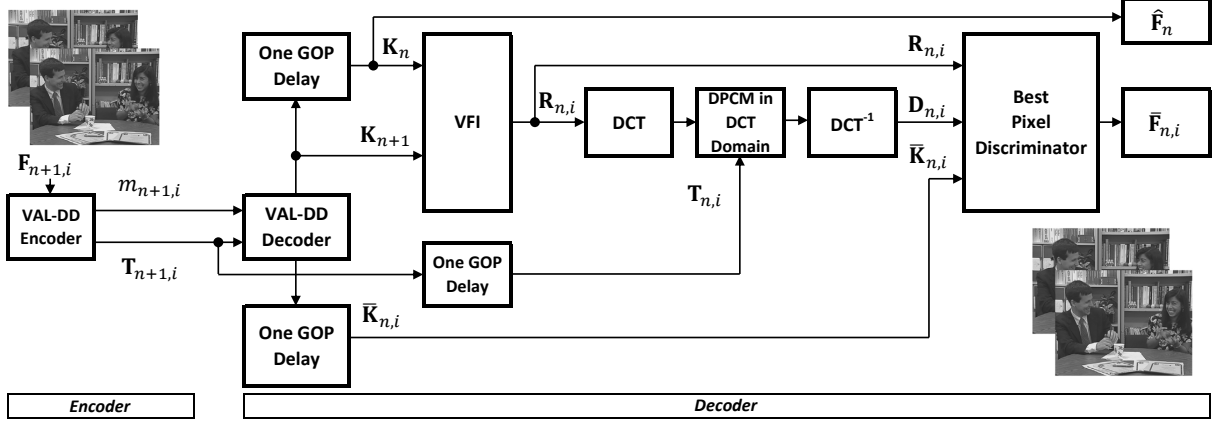


FIGURE 2. Block diagram of the distributed VAL-VFI algorithm. The VAL-DD decoder has optional IDA reconstruction.

- We prove that using a linear 2D-DCT measurement matrix allows temporal DPCM at the decoder by simply filtering and mixing transform coefficients from the key and non-key frames.
- Coupled with the above, and using a plug-and-play, CNN-based video frame interpolation module, we reach state-of-the-art PSNR and MS-SSIM performance, with an execution time that is two orders of magnitude lower than current state-of-the-art methods.
- Additionally, we can reconstruct the video using the recently proposed iterative denoising algorithm (IDA) [12] that can compressively reconstruct a full image from the adaptively and deterministically sensed blocks, to improve the video quality.

II. RELATED WORK

Fowler and Mun [27] proposed the MC-BCS-SPL algorithm which incorporates block-based motion estimation (ME) and compensation (MC) at the decoder. In a GOP with P pictures, they recover the first $P/2$ frames with forward reconstruction starting from the intra-frame, and the remaining frames, by reconstructing them from the reference frame in the next GOP. They then refine the frames by bi-directional prediction from the previous and following frames. Chen et al. [28] took inspiration from this framework and proposed multi-hypothesis predictions (BCS-SPL-MH) as an improvement for both still images and video. An initial reconstruction is performed using standard BCS-SPL [27], and weighted Tikhonov regularization is then used to form predictions of the residual to iteratively improve the reconstruction.

Recently, Zhao et al. [19] proposed a two-phase hybrid intra-frame, inter-frame algorithm. The first phase exploits spatial correlation to produce high-quality reference frames. In the second, the reweighted sparsity of the residual difference between frames is recovered using an algorithm based on split Bregman iteration. Experimental results are presented for the first 16 frames of six popular common CIF video sequences. The GOP consists of an intra-frame followed by seven inter-frames. Block-based sensing is assumed

using Gaussian random projections on 32×32 pixel blocks. Key frames are sensed at a compression ratio of 0.7 and non-key frames at 0.2. Multi-hypothesis prediction is used to reconstruct the inter-frames. The proposed reweighted residual sparsity (RRS) scheme is compared against four representative video CS reconstruction methods, and was shown to achieve state-of-the-art performance. However, the reconstruction time per frame was reported to exceed 5 minutes.

SGS-OF [3] is closest to our work, both in terms of concept and results. The authors adopt a GOP with size 8 and compressively sense key and non-key frames with compression ratios 0.7 and 0.1. They propose a structural group sparsity (SGS) model and employ the alternating direction method of multipliers (ADMM) variant of the augmented Lagrangian method (ALM), to reconstruct the independent frames, and then use the Coarse-to-Fine optical flow (OF) method to create a fused image using the forward and backward OF motion estimates. Finally they use the BCS-SPL [29] algorithm to refine the original reconstruction using residual estimation and compensation. The authors investigate both Gaussian and partial DCT measurement matrices and report large gains with the deterministic Partial DCT matrices. The authors quote a reconstruction time of around 15s per frame using the partial DCT sensing matrix.

III. DISTRIBUTED VIDEO COMPRESSIVE SENSING

Inspired by distributed video compressive sensing techniques, we develop the VAL framework described in this section and evaluate it empirically in section IV. The block diagram of the proposed VAL-VFI algorithm is shown in figure 2. The GOP structure in figure 3 is adopted wherein key frames are sensed with a high average key compression ratio $\delta_K = M/N$ so that the reconstructed quality is high, where N is the number of pixels and M the number of measurements. Non-key frames are sensed with a substantially lower $\delta_{\bar{K}}$. We place the key-frames at the start of the GOPs and then predict the non-key-frames from the key-frames in the current and following GOP, using VFI.

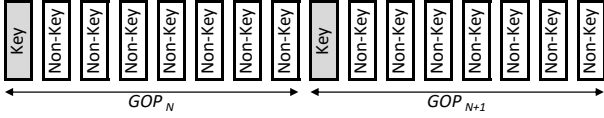


FIGURE 3. GOP Structure. N is the Group of Pictures number.

The encoder captures frames $\mathbf{F}_{n+1,i}$ using two adaptive VAL-DD algorithms inspired by the AL-DCT-DD algorithm in [12]. \mathbf{F}_{n+1} is the Key frame in GOP $n+1$. $\mathbf{F}_{n+1,i}$ is the i -th non-key frame in GOP $n+1$, $i = 2..g$ where g is the GOP size. The encoder then transmits the compressively sensed 2D-DCT transform coefficients $\mathbf{T}_{n+1,i}$ and the number of transform coefficients per block $m_{n+1,i}$ sensed in the i -th frame of the GOP.

The decoder decodes the key and non-key frames, in real-time, using the inverse 2D DCT in the VAL-DD decoder, and buffers one GOP worth of transform coefficients and reconstructed non-key frames. This is necessary because the VFI algorithm requires the key frame in the current GOP \mathbf{K}_n and that in the following GOP \mathbf{K}_{n+1} , besides the i -th non-key frame $\bar{\mathbf{K}}_{n,i}$ in the current GOP.

The VFI block uses the two key frames \mathbf{K}_n and \mathbf{K}_{n+1} to interpolate the non-key frames $\mathbf{R}_{n,i}$ in between. The decoder then computes the temporal DPCM in the transform domain to predict the received frame from the reference frame $\mathbf{R}_{n,i}$ and non-key transform coefficients $\mathbf{T}_{n,i}$. The DPCM output $\mathbf{D}_{n,i}$ is then compared with $\mathbf{R}_{n,i}$ in the *best pixel discriminator* block that outputs $\mathbf{D}_{n,i}$ or $\bar{\mathbf{K}}_{n,i}$ to produce the reconstructed non-key frame $\bar{\mathbf{F}}_{n,i}$. The reconstructed key frame $\hat{\mathbf{F}}_n$ is equal to \mathbf{K}_n .

Better quality can be achieved if the VAL-DD reconstruction is carried out using the IDA algorithm with the DnCNN denoiser [12].

A. ADAPTIVE BLOCK COMPRESSIVE SENSING

At the encoder, transform coefficients (TC) are sensed in two phases. Measurements from the first phase are used to estimate the number of adaptive measurements in the second phase. We propose two improved versions of the AL-DCT-DD algorithm in [12]; threshold over the whole image (THI) and mixed-mode DCT domain (MDD).

THI is defined in algorithm 1. It collects half the TCs equally from all blocks in phase one. These are then used to estimate the number of phase-2 coefficients based on the proportion of the largest phase-1 coefficients from all blocks in the image that fall in the current block.

When compressively sensing successive non-key frames in a video sequence, one would have the benefit of having collected significantly more TCs per block from the key frame, which is sensed at a substantially higher rate. We thus propose another algorithm that adapts the phase-two measurements based on the reference key-frame phase-1 TCs, but replacing the low-pass TCs with the phase-1 TCs of the current frame. We refer to this as the mixed-mode DCT domain (MDD) as described in algorithm 2).

Algorithm 1: THI

Input: Image \mathcal{I} , compression factor $C_F = N/M$, block size B , image width W , image height H .

Output: Number of measurements m_i per block i , m_i measurements per block.

- 1 Crop and partition, \mathcal{I} into $n_B = \lfloor H/B \rfloor \cdot \lfloor W/B \rfloor$, $B \times B$ blocks;
 - 2 Calculate the number of non-adaptive, phase-1 measurements per block $m_i^1 = \lfloor B^2 / (2 \cdot C_F) \rfloor$;
 - 3 Collect m_i^1 low-pass 2D DCT coefficients in zigzag order from each block;
 - 4 Sort all phase-1 coefficients in descending order of absolute magnitude;
 - 5 Set a threshold T_I which is equal to the absolute value of the $(M/4)$ -th largest coefficient in the sorted list of coefficients, where $M = (H \times W) / C_F$;
 - 6 Calculate m_i^T , the number of coefficients in each block whose absolute value exceeds T_I ;
 - 7 Set the number of coefficients to collect from each block in phase 2, m_i^2 , to $2 \times m_i^T$;
 - 8 Collect m_i^2 additional coefficients as required;
 - 9 Output $m_i = m_i^1 + m_i^2$, the number of measurements per block;
 - 10 Output the m_i measurements per block.
-

Algorithm 2: MDD

Input: Image \mathcal{I} , transform coefficients of reference image TC_{Ref} , compression factor $C_F = N/M$, block size B , image width W , image height H .

Output: Number of measurements m_i per block i , m_i measurements per block.

- 1 Crop and partition \mathcal{I} into $n_B = \lfloor H/B \rfloor \cdot \lfloor W/B \rfloor$, $B \times B$ blocks;
 - 2 Calculate the number of non-adaptive measurements per block $m_i^1 = \lfloor B^2 / (2 \cdot C_F) \rfloor$;
 - 3 Collect m_i^1 low-pass 2D DCT coefficients in zigzag order from each block;
 - 4 Replace the m_i^1 low pass coefficients in TC_{Ref} by the TCs collected in step 3;
 - 5 Set m_i^2 equal to the number of largest M transform coefficients in TC_{Ref} by absolute value, that fall in each block i ;
 - 6 Collect m_i^2 additional coefficients as required;
 - 7 Output $m_i = m_i^1 + m_i^2$, the number of measurements per block;
 - 8 Output the m_i measurements per block.
-

B. IDA RECONSTRUCTION

The IDA algorithm proposed in [12] can reconstruct adaptive block based images sensed using the deterministic 2D DCT measurement matrix. We propose to use IDA to increase the PSNR and MS-SSIM of the reconstructed video. The IDA algorithm is an iterative thresholding algorithm that uses the CNN-based, DnCNN denoiser [30].

C. VIDEO FRAME INTERPOLATION

VFI has been extensively studied over the past decades to up-sample the frame rate of video content to match the ever increasing video monitor frame rates and produce smoother

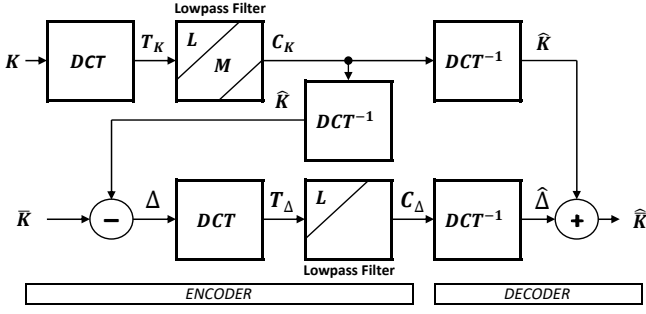


FIGURE 4. Non-distributed hybrid DPCM/DCT coder.

playback and slow-motion effects. Recently, CNNs have been leveraged to generate interpolated frames in real-time [31]. One of the better performing CNN-based systems is DAIN [25] which can interpolate frames in real-time. Key frames are encoded with a higher quality (i.e., with lower compression) than non-key frames. Therefore, we leverage video frames interpolated from two key frames by DAIN [25] as high-quality estimates of non-key frames. We then use the VFI output frame $\mathbf{R}_{n,i}$ as the input to the temporal DPCM block, which continues to improve video quality.

D. DIFFERENTIAL PULSE CODE MODULATION

Temporal DPCM exploits correlation between frames. Consider the hybrid DPCM/DCT codec in figure 4. A $B \times B$ pixel block from key-frame \mathbf{K} is transformed using a 2D DCT operation generating $B \times B$ transform coefficients \mathbf{T}_K . We define the compressive L-DCT-ZZ operation, as that operation that retains $(L+M)$ lowpass transform coefficients in JPEG [32] zigzag order. L is the number of transform coefficients retained in a non-key frame and M are the number of extra mid-band DCT coefficients retained in a key-frame, over and above those in the non-key frame. The resulting \mathbf{C}_K transform coefficients are transmitted to the decoder, where an inverse 2D DCT reconstructs the key frame estimate $\hat{\mathbf{K}}$.

To exploit the correlation between a key frame block and a non-key frame block $\bar{\mathbf{K}}$, the key frame block estimate $\hat{\mathbf{K}}$ is subtracted from the non-key frame block. The resulting difference block Δ is transformed using the 2D DCT, generating transform coefficients \mathbf{T}_Δ which are lowpass filtered, retaining only L upper triangular transform coefficients \mathbf{C}_Δ . At the decoder, \mathbf{C}_Δ is inverse transformed to reconstruct an estimate of the difference block $\hat{\Delta}$ that is added to the frame block estimate $\hat{\mathbf{K}}$ to estimate the non-key frame block $\hat{\hat{\mathbf{K}}}$.

Let the key frame pixel block \mathbf{K} be arranged into a column vector \mathbf{k} . The linear unitary 2D DCT transform \mathbf{D} then transforms \mathbf{k} into the column vector of TCs \mathbf{t}_K

$$\mathbf{t}_K = \mathbf{D}\mathbf{k} \quad (2)$$

where \mathbf{D} is the $N \times N$ transform matrix and $N = B \times B$. The lowpass filtering operation is accomplished by element-wise multiplication (denoted by \odot) of \mathbf{t}_K with a matrix consisting of $L+M$ 1's in the upper left hand triangle and 0's

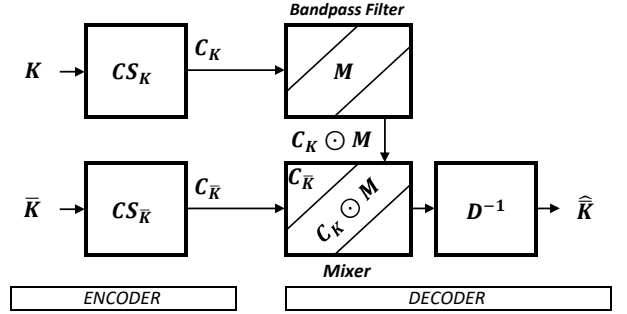


FIGURE 5. Distributed compressive DPCM in the DCT domain. CS_K and $\text{CS}_{\bar{K}}$ represent the CS operations on the key and non-key blocks.

elsewhere, arranged as a vector \mathbf{f}_{L+M} , such that the L-DCT-ZZ vectorized coefficients of the key frame \mathbf{c}_K are given by

$$\begin{aligned} \mathbf{c}_K &= \mathbf{t}_K \odot \mathbf{f}_{L+M} \\ &= (\mathbf{D}\mathbf{k}) \odot \mathbf{f}_{L+M} \\ &= (\mathbf{D}\mathbf{k}) \odot \mathbf{f}_L + (\mathbf{D}\mathbf{k}) \odot \mathbf{f}_M \end{aligned} \quad (3)$$

The L-DCT-ZZ vectorized coefficients of the difference block are given by

$$\begin{aligned} \mathbf{c}_\Delta &= [\mathbf{D}(\bar{\mathbf{k}} - \mathbf{D}^{-1}\mathbf{c}_K)] \odot \mathbf{f}_L \\ &= [\mathbf{D}\bar{\mathbf{k}} - \mathbf{c}_K] \odot \mathbf{f}_L \\ &= (\mathbf{D}\bar{\mathbf{k}}) \odot \mathbf{f}_L - (\mathbf{D}\mathbf{k}) \odot \mathbf{f}_{L+M} \odot \mathbf{f}_L \\ &= (\mathbf{D}\bar{\mathbf{k}}) \odot \mathbf{f}_L - (\mathbf{D}\mathbf{k}) \odot \mathbf{f}_L \end{aligned} \quad (4)$$

since $\mathbf{f}_{L+M} = \mathbf{f}_L + \mathbf{f}_M$ and $(\mathbf{f}_L + \mathbf{f}_M) \odot \mathbf{f}_L = \mathbf{f}_L$, given that \mathbf{f}_L and \mathbf{f}_M are disjoint ($\mathbf{f}_L \cap \mathbf{f}_M = \{\mathbf{0}\}$).

Equation (3) shows that the key frame entails transmitting the L lowpass and M mid-band L-DCT-ZZ coefficients. Equation (4) shows that the DPCM difference transform coefficients \mathbf{c}_Δ are composed of the lowpass coefficients of the non-key frame from which are subtracted from the lowpass coefficients of the key frame. Therefore, the encoder can be simplified to just two L-DCT-ZZ encoders one for the key frames retaining $(L+M)$ transform coefficients and one for the non-key frames retaining just L coefficients. The difference block coefficients \mathbf{c}_Δ can then be calculated at the decoder by subtracting the key frame lowpass coefficients $(\mathbf{D}\mathbf{k}) \odot \mathbf{f}_L$ from the non-key frame lowpass coefficients $(\mathbf{D}\bar{\mathbf{k}}) \odot \mathbf{f}_L$.

E. REAL-TIME RECONSTRUCTION

The VAL-DD encoder transmits the transform coefficients and the number m_i of transform coefficients per block to the decoder. For the key frames, the decoder then reconstructs each image block using the inverse linear 2D-DCT. The reconstructed key block arranged as a column vector is given by

$$\hat{\mathbf{k}} = \mathbf{D}^{-1}\mathbf{c}_k \quad (5)$$

This can be achieved in real-time using matrix multiplication or fast implementations of the inverse 2D-DCT.

The non-key frame can be computed by first calculating \mathbf{c}_Δ at the encoder as described in III-D, multiplying it by the

inverse 2D DCT matrix \mathbf{D}^{-1} to generate the difference block and then adding it to key frame. In vector form

$$\hat{\mathbf{k}} = \mathbf{D}^{-1}\mathbf{c}_\Delta + \hat{\mathbf{k}} \quad (6)$$

However, we can also write

$$\begin{aligned} \hat{\mathbf{k}} &= \mathbf{D}^{-1}(\mathbf{c}_\Delta + \mathbf{c}_\mathbf{K}) \\ &= \mathbf{D}^{-1}[(\mathbf{D}\bar{\mathbf{k}}) \odot \mathbf{f}_L + (\mathbf{D}\mathbf{k}) \odot \mathbf{f}_M] \end{aligned} \quad (7)$$

Thus the non-key frame can also be computed by first mixing (adding) the mid-band transform coefficients of the key frame to the lowpass transform coefficients of the non-key frame and calculating the inverse 2D DCT transform as shown in the distributed version of the DPCM operation in figure 5. Note that in figure 2, \mathbf{F}_{n+1} corresponds to key frames \mathbf{K} in figure 5, and $\mathbf{F}_{n+1,i}$ to non-key frames $\bar{\mathbf{K}}$ for $i > 0$.

F. BEST PIXEL DISCRIMINATOR

In unchanging parts of a frame, selecting key-frame blocks results in a higher-quality rendition. VFI results in estimating high-quality key-frame blocks and the subsequent DPCM process combines them with the low-pass current blocks. If the VFI is not accurate, image artefacts appear in the output blocks and this occurs where the image is changing most dynamically.

Following reconstruction of the current non-key frame and VFI from the key frame, we have three versions of the reconstructed frame; $\bar{\mathbf{K}}_{n,i}$ is low resolution non-key frame with no artefacts, $\mathbf{R}_{n,i}$ is the higher resolution VFI predicted frame but with the possibility of image artefacts, and $\mathbf{D}_{n,i}$ which is the DPCM output that may also have visible artefacts. To reduce the visibility of VFI artefacts, one option would be to average the two reconstructions together and this will indeed result in a better PSNR and MS-SSIM.

A second option is to compare the pixels at location (i, j) in both $\mathbf{R}_{n,i}$ and $\mathbf{D}_{n,i}$ and if the modulus of the difference $|\mathbf{R}_{n,i} - \mathbf{D}_{n,i}|$ is less than a threshold T_D then the output pixel is set to $\mathbf{D}_{n,i}$; otherwise it is set to $\bar{\mathbf{K}}_{n,i}$.

This selection operation was found to improve the output quality considerably. The value of T_D was investigated empirically. A value of $T_D = 25$ was found to give good results with this best pixel discriminator (BPD) block in the VAL-VFI versions of our algorithms, whereas $T_D = 10$ gave the best results with VAL-IDA-VFI.

The BPD results in lowpass pixels at the edges of moving objects in the current output frame. However the visual quality is still better as the human vision system is less sensitive to errors at moving boundaries.

G. VAL-VFI PARAMETERS

The VAL-VFI framework is characterised by a number of parameters that have to be taken into consideration, ideally optimized, namely: DCT block size; GOP size; compression ratio (or subrate) $\delta = M/N$, for key and non-key frames; IDA damping factor and iterations, if used; and BPD threshold T_D .

IV. SIMULATION RESULTS

The simulations in this section were executed on a server equipped with an Intel Xeon CPU E5-160 v3 clocked at 3.50 GHz, with 32GB of RAM, running MATLAB version 2019a on Linux 18.04. IDA requires the D-AMP-Toolbox from [33]. The DnCNN code and models were downloaded from [34] and require the MatConvNet [35] package from [36]. The DAIN code was downloaded from the author's site [37]. We compiled it with Pytorch version 1.1 and it runs under Python 3.7.9. The VAL-IDA code exchanges Key and non-Key frames with DAIN at run time, using a file-based interface. The source code for this paper is available at: <https://github.com/jzamm/val>. Note that the algorithms presented in this paper extend to higher resolution images, the included code can be utilized without any modifications. The image test sets below were chosen to compare with published work, claiming SOTA performance, for which the source code was not available.

The VAL-VFI and VAL-IDA-VFI algorithms were compared with three algorithms in the literature; ME/MC [28], RRS [8] and SGS-OF [3]. Six popular CIF video sequences were used for testing as in [3]. We refer to this set as VidSet6. The first seventeen frames of VidSet6 were used with the seventeenth frame used by VFI to compute key frames in the second GOP, but PSNR and MS-SSIM [26] results are only reported for the luminance (Y) plane of the first sixteen frames. The simulation uses blocks of size $B = 16$. The key compression ratio δ_K , non-key compression ratio $\delta_{\bar{K}}$ and GOP size G are related by the following equation:

$$\frac{\delta_K + (G - 1)\delta_{\bar{K}}}{G} = 0.175 \quad (8)$$

This ensures a constant average number of CS measurements per GOP. G , δ_K and $\delta_{\bar{K}}$ were initially set to 8, 0.7 and 0.1 respectively and then varied to optimize PSNR and MS-SSIM results as indicated below. Note that the higher the compression ratio, the more measurements are collected by the compressive sensing.

The original ME/MC code from [38] and RRS code from [19] were modified to set the measurement matrix to the same DCT measurement matrix used by our algorithms. The use of the low-pass DCT measurement matrix improves the results of both ME/MC and RRS over the respective published results. SGS-OF code was not available and therefore, the SGS-OF results in table 1 are from the original paper in [3].

A. PSNR AND MS-SSIM

The average PSNR and MS-SSIM results of VAL-VFI and VAL-IDA-VFI are compared with ME/MC, RRS and SGS-OF in table 1. When the GOP size is 8, and the key and non-key frame compression ratios are 0.7 and 0.1 respectively, VAL-VFI exceeds the performance of ME/MC, RRS and SGS-OF by 2.96 dB, 3.80 dB and 0.40 dB respectively. It also exceeds the MS-SSIM of ME/MC and RRS by 0.0199 and 0.0083, but is 0.0011 short of SGS-OF. IDA reconstruction

Video Sequence	ME/MC GOP=8 $\delta_K = 0.7$	RRS GOP=8 $\delta_K = 0.7$	SGS-OF GOP=8, $\delta_K = 0.7$	VAL-VFI GOP=8 $\delta_K = 0.7$	VAL-IDA-VFI GOP=8 $\delta_K = 0.7$	VAL-IDA-VFI GOP=8 $\delta_K = 0.4$	VAL-VFI GOP=4 $\delta_K = 0.5$	VAL-IDA-VFI GOP=4 $\delta_K = 0.5$
Paris	29.63, 0.9872	27.07, 0.9853	32.00, 0.9946	32.28, 0.9933	33.82 , 0.9932	31.79, 0.9938	31.26, 0.9941	33.72, 0.9953
Foreman	32.85, 0.9829	36.51, 0.9943	37.20 , 0.9952	35.45, 0.9903	37.19, 0.9891	37.10, 0.9924	35.51, 0.9916	36.61, 0.9920
Coastguard	30.14, 0.9470	31.20, 0.9535	32.40, 0.9692	32.35, 0.9680	32.70, 0.9670	32.10, 0.9745	34.31, 0.9832	34.49 , 0.9833
Hall	41.12, 0.9960	35.68, 0.9947	40.30, 0.9953	42.02, 0.9959	42.21 , 0.9946	41.19, 0.9951	41.05, 0.9959	41.78, 0.9959
Mobile	21.39, 0.9059	23.96, 0.9610	27.13, 0.9897	28.33, 0.9900	28.75, 0.9896	27.33, 0.9890	27.82, 0.9903	29.45 , 0.9929
News	38.39, 0.9967	34.11, 0.9965	39.88, 0.9978	40.91, 0.9974	42.18 , 0.9973	41.11, 0.9978	40.77, 0.9977	41.39, 0.9978
Average	32.26, 0.9693	31.42, 0.9809	34.82, 0.9903	35.22, 0.9892	36.14, 0.9885	35.10, 0.9904	35.12, 0.9921	36.24 , 0.9929

TABLE 1. VAL-VFI and VAL-IDA-VFI algorithms compared with ME/MC [28], RRS [8] and SGS-OF [3]. PSNR on the left, SSIM on the right. Best results in bold.

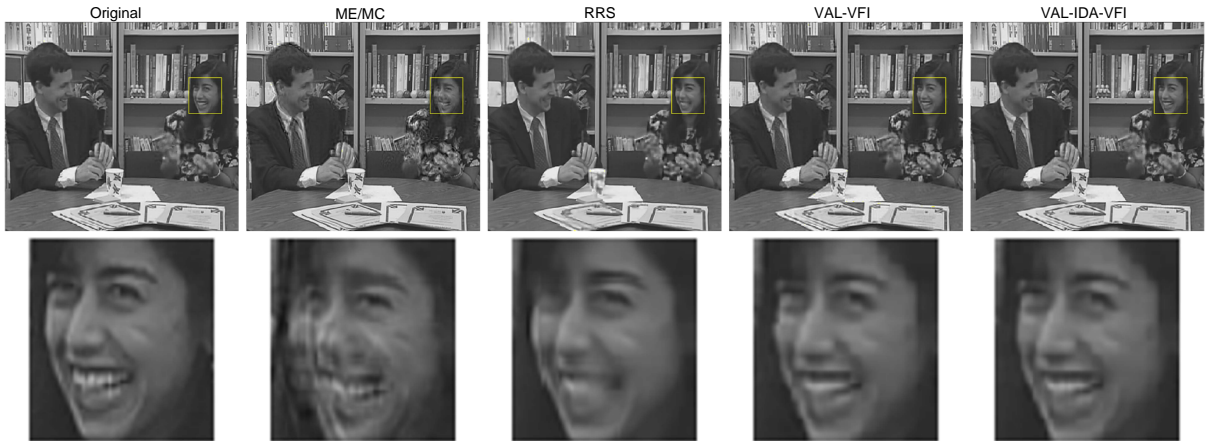


FIGURE 6. Frame 14 of the Paris sequence output Original, and reconstructed by ME/MC, RRS, VAL-VFI and VAL-IDA-VFI.

improves the VAL-VFI PSNR by 0.92 dB but decreases MS-SSIM marginally by 0.0007.

The GOP and δ_K values were then varied to optimise the VAL-VFI and VAL-IDA-VFI performance. When GOP=8, $\delta_K = 0.4$ and $\delta_{\bar{K}} = 0.1429$ as computed by equation (8), VAL-IDA-VFI exceeds the state-of-the-art PSNR and MS-SSIM performance of SGS-OF by 0.28 dB and 0.0001. If the GOP size is reduced to 4, $\delta_K = 0.5$ and $\delta_{\bar{K}} = 0.0667$, the VAL-VFI PSNR and MS-SSIM exceed that of SGS-OF by 0.30 dB and 0.0018. VAL-IDA-VFI with GOP=4, $\delta_K = 0.5$ and $\delta_{\bar{K}} = 0.0667$ achieves our best results and improves VAL-VFI PSNR and MS-SSIM by 1.12 dB and 0.0008 respectively.

Figure 7 compares the PSNR of the Y component of the first 16 frames of the VidSet6 sequences. The GOP size is 8 in all cases except for VAL-IDA-VFI* for which the GOP size is 4. The compression ratio of the key frame is 0.7 for ME/MC, RRS and SGS-OF whereas it is 0.6 for VAL-IDA-VFI and 0.5 for VAL-IDA-VFI*. The average compression ratio over the whole GOP is 0.175 in all cases. As can be seen from the figure, the non-key PSNR for VAL-IDA-VFI* is superior to the other algorithms in the Paris, Coastguard and Mobile

sequences. VAL-IDA-VFI has the best non-key PSNR in the Hall and News sequences whereas SGS-OF prevails in the Foreman sequence. The variability of the PSNR is least for VAL-IDA-VFI* with the key compression ratio equal to 0.5.

B. VISUAL QUALITY AND EXECUTION TIME

The visual quality of the fourteenth frame of the Paris sequence produced by the VAL-VFI and VAL-IDA-VFI algorithms is compared with the original frame and the output of ME/MC and RRS algorithms in figure 6. VAL-VFI and VAL-IDA-VFI (GOP = 4, $\delta_K = 0.5$, $\delta_{\bar{K}} = 0.0667$) both have better rendition than ME/MC and RRS, with no artefacts like ME/MC and with sharper rendition. VAL-IDA-VFI improves on the VAL-VFI quality. The non-optimized VAL-VFI reconstructs a frame in around 190ms, VAL-IDA-VFI in 2.1 seconds (20 iterations of the DnCNN algorithm, PSNR = 36.15 dB, MS-SSIM = 0.9928), ME/MC in 15s and RRS in 557s. SGS-OF is reported in [3] to reconstruct a frame in 15s on a server with equivalent processing power.

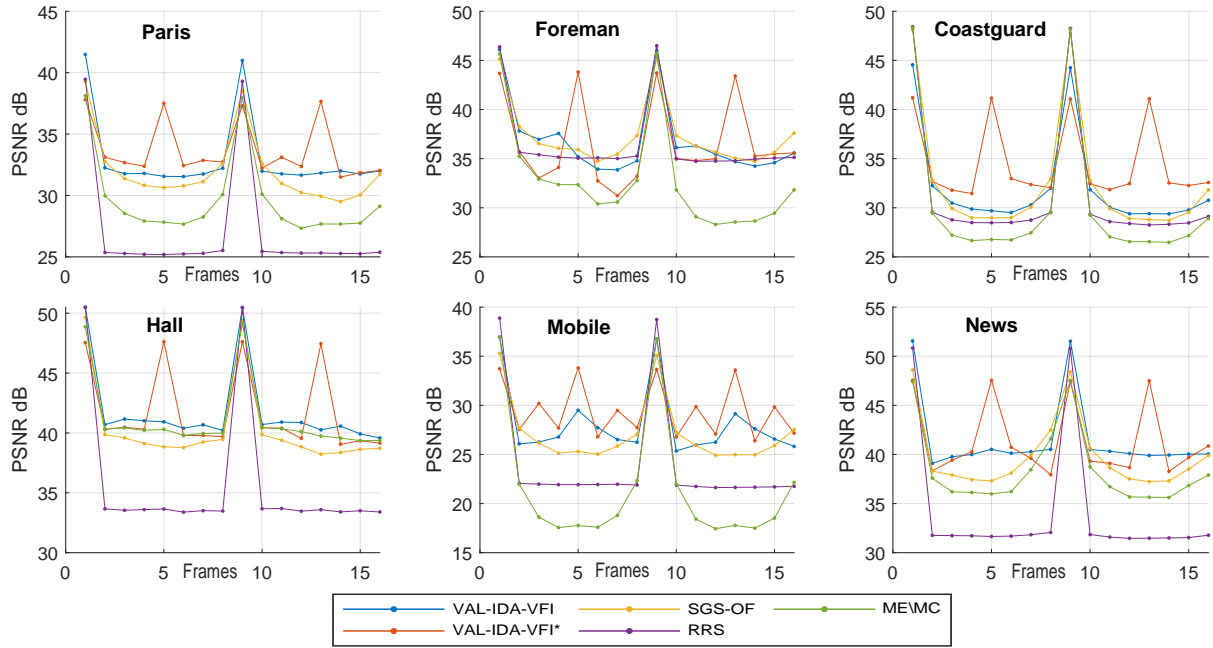


FIGURE 7. Comparing the PSNR for the first 16 frames of VidSet6 compressed with VAL-IDA-VFI, ME/MC, RRS and SGS-OF, with GOP = 8, VAL-IDA-VFI* with GOP=4. The average compression ratio is 0.175 across the GOP.

V. CONCLUSION

We have proposed the VAL-VFI and VAL-IDA-VFI algorithms that exploit adaptive, block-based compressive sensing of video frames in the spatial domain, using deterministic DCT matrices. The reconstruction quality of the compressively sensed frames can be enhanced using an iterative denoising algorithm.

Our algorithms exploit temporal correlation at the encoder using the MDD adaptivity estimation algorithm to match the compressive sensing ratio with the underlying block sparsity. At the decoder we exploit temporal correlation using a GOP structure and a video frame interpolation CNN to predict non-key frames from higher-quality key frames. The quality of the VFI frames is then enhanced by performing temporal DPCM at the decoder. Finally, a best pixel discriminator can select the best pixel from the DPCM output or the reconstructed non-key frame, depending on the pixel error between the VFI prediction and the DPCM reconstruction. Simulation results show that our algorithms achieve state-of-the-art performance. The improvement in performance is shown in figure 1.

Future work can study VAL-VFI in an end-to-end transmission system, digitally encoding the adaptive measurements prior to transmission.

REFERENCES

- [1] D. Slepian and J. Wolf, "Noiseless coding of correlated information sources," *IEEE Transactions on information Theory*, vol. 19, no. 4, pp. 471–480, 1973.
- [2] A. Wyner and J. Ziv, "The rate-distortion function for source coding with side information at the decoder," *IEEE Transactions on information Theory*, vol. 22, no. 1, pp. 1–10, 1976.
- [3] J. Chen, Z. Chen, K. Su, Z. Peng, and N. Ling, "Video compressed sensing reconstruction based on structural group sparsity and successive approximation estimation model," *Journal of Visual Communication and Image Representation*, vol. 66, p. 102734, 2020.
- [4] E. J. Candes, J. Romberg, and T. Tao, "Robust uncertainty principles: exact signal reconstruction from highly incomplete frequency information," *IEEE Transactions on Information Theory*, vol. 52, no. 2, pp. 489–509, Feb 2006.
- [5] D. L. Donoho, "Compressed sensing," *IEEE Transactions on Information Theory*, vol. 52, no. 4, pp. 1289–1306, April 2006.
- [6] V. K. Goyal, A. K. Fletcher, and S. Rangan, "Compressive sampling and lossy compression," *IEEE Signal Processing Magazine*, vol. 25, no. 2, pp. 48–56, 2008.
- [7] S. Mun and J. E. Fowler, "Block compressed sensing of images using directional transforms," in *2010 Data Compression Conference*, March 2010, pp. 547–547.
- [8] C. Zhao, S. Ma, J. Zhang, R. Xiong, and W. Gao, "Video compressive sensing reconstruction via reweighted residual sparsity," *IEEE Transactions on Circuits and Systems for Video Technology*, vol. 27, no. 6, pp. 1182–1195, 2016.
- [9] Lu Gan, "Block compressed sensing of natural images," in *2007 15th International Conference on Digital Signal Processing*, July 2007, pp. 403–406.
- [10] J. E. Fowler, S. Mun, E. W. Tramel et al., "Block-based compressed sensing of images and video," *Foundations and Trends in Signal Processing*, vol. 4, no. 4, pp. 297–416, 2012.
- [11] R. Baraniuk, M. Davenport, R. DeVore, and M. Wakin, "A simple proof of the restricted isometry property for random matrices," *Constructive Approximation*, vol. 28, no. 3, pp. 253–263, 2008.
- [12] J. Zammit and I. J. Wassell, "Adaptive block compressive sensing: Toward a real-time and low-complexity implementation," *IEEE Access*, vol. 8, pp. 120 999–121 013, 2020.
- [13] S. G. Mallat and Z. Zhang, "Matching pursuits with time-frequency dictionaries," *IEEE Transactions on signal processing*, vol. 41, no. 12, pp. 3397–3415, 1993.
- [14] D. Baron, S. Sarvotham, and R. G. Baraniuk, "Bayesian compressive sensing via belief propagation," *IEEE Transactions on Signal Processing*, vol. 58, no. 1, pp. 269–280, 2009.
- [15] D. L. Donoho, A. Maleki, and A. Montanari, "Message-passing algorithms for compressed sensing," *Proceedings of the National Academy of Sciences*, vol. 106, no. 45, pp. 18 914–18 919, 2009.

- [16] C. A. Metzler, A. Maleki, and R. G. Baraniuk, "From denoising to compressed sensing," *IEEE Transactions on Information Theory*, vol. 62, no. 9, pp. 5117–5144, 2016.
- [17] A. Mousavi, A. B. Patel, and R. G. Baraniuk, "A deep learning approach to structured signal recovery," in *2015 53rd Annual Allerton Conference on Communication, Control, and Computing (Allerton)*. IEEE, 2015, pp. 1336–1343.
- [18] C. Metzler, A. Mousavi, and R. Baraniuk, "Learned d-amp: Principled neural network based compressive image recovery," in *Advances in Neural Information Processing Systems*, 2017, pp. 1772–1783.
- [19] C. Zhao, J. Zhang, R. Wang, and W. Gao, "Cream: Cnn-regularized admm framework for compressive-sensed image reconstruction," *IEEE Access*, vol. 6, pp. 76 838–76 853, 2018.
- [20] K. Kulkarni, S. Lohit, P. Turaga, R. Kerviche, and A. Ashok, "Reconnet: Non-iterative reconstruction of images from compressively sensed measurements," in *Proceedings of the IEEE Conference on Computer Vision and Pattern Recognition*, 2016, pp. 449–458.
- [21] W. Shi, F. Jiang, S. Zhang, and D. Zhao, "Deep networks for compressed image sensing," in *2017 IEEE International Conference on Multimedia and Expo (ICME)*. IEEE, 2017, pp. 877–882.
- [22] J. Zhang and B. Ghanem, "Ista-net: Interpretable optimization-inspired deep network for image compressive sensing," in *Proceedings of the IEEE conference on computer vision and pattern recognition*, 2018, pp. 1828–1837.
- [23] W. Shi, F. Jiang, S. Liu, and D. Zhao, "Scalable convolutional neural network for image compressed sensing," in *Proceedings of the IEEE Conference on Computer Vision and Pattern Recognition*, 2019, pp. 12 290–12 299.
- [24] W. Shi, S. Liu, F. Jiang, and D. Zhao, "Video compressed sensing using a convolutional neural network," *IEEE Transactions on Circuits and Systems for Video Technology*, 2020.
- [25] W. Bao, W.-S. Lai, C. Ma, X. Zhang, Z. Gao, and M.-H. Yang, "Depth-aware video frame interpolation," in *Proceedings of the IEEE Conference on Computer Vision and Pattern Recognition*, 2019, pp. 3703–3712.
- [26] Z. Wang, E. P. Simoncelli, and A. C. Bovik, "Multiscale structural similarity for image quality assessment," in *The Thrity-Seventh Asilomar Conference on Signals, Systems & Computers*, 2003, vol. 2. Ieee, 2003, pp. 1398–1402.
- [27] S. Mun and J. E. Fowler, "Residual reconstruction for block-based compressed sensing of video," in *2011 Data Compression Conference*. IEEE, 2011, pp. 183–192.
- [28] C. Chen, E. W. Tramel, and J. E. Fowler, "Compressed-sensing recovery of images and video using multihypothesis predictions," in *2011 Conference Record of the Forty Fifth Asilomar Conference on Signals, Systems and Computers (ASILOMAR)*, Nov 2011, pp. 1193–1198.
- [29] S. Mun and J. E. Fowler, "Block compressed sensing of images using directional transforms," in *2009 16th IEEE international conference on image processing (ICIP)*. IEEE, 2009, pp. 3021–3024.
- [30] K. Zhang, W. Zuo, Y. Chen, D. Meng, and L. Zhang, "Beyond a gaussian denoiser: Residual learning of deep cnn for image denoising," *IEEE Transactions on Image Processing*, vol. 26, no. 7, pp. 3142–3155, 2017.
- [31] S. Nah, R. Timofte, S. Gu, S. Baik, S. Hong, G. Moon, S. Son, and K. Mu Lee, "Ntire 2019 challenge on video super-resolution: Methods and results," in *Proceedings of the IEEE Conference on Computer Vision and Pattern Recognition Workshops*, 2019, pp. 0–0.
- [32] I. IEC, "Information technology-digital compression and coding of continuous-tone still images: Requirements and guidelines," *Standard, ISO IEC*, pp. 10 918–1, 1994.
- [33] D-AMP Toolbox. (08-Jul-2017) https://github.com/ricedsp/d-amp_toolbox. Accessed May. 05, 2019. [Online]. Available: https://github.com/ricedsp/D-AMP_Toolbox
- [34] DnCNN source code. (08-Jul-2017) <https://github.com/cszn/dncnn>. Accessed May. 05, 2019. [Online]. Available: <https://github.com/cszn/DnCNN>
- [35] A. Vedaldi and K. Lenc, "Matconvnet – convolutional neural networks for matlab," in *Proceeding of the ACM Int. Conf. on Multimedia*, 2015.
- [36] Vedaldi, A. and Lenc, K., "Matconvnet," 17-Aug-2017, accessed May. 05, 2019. [Online]. Available: <https://www.vlfeat.org/matconvnet/>
- [37] B. Wenbo. (2020) Dain. Accessed, June. 05, 2020. [Online]. Available: <https://github.com/baowenbo/DAIN>
- [38] J.E. Fowler. (31-Jan-2017) Mc-bcs-spl version 1.1-1. Accessed May. 05, 2019. [Online]. Available: <http://www.ece.msstate.edu/~fowler/BCSSPL>



JOSEPH ZAMMIT received the B.Sc. degree in Communications and Computer Engineering from the University of Malta, Msida, Malta, in 2012, the M.Sc. degree in Wireless and Optical Communications, from University College London, London, U.K., in 2013, and is a Ph.D. candidate at the Computer Laboratory, University of Cambridge, Cambridge, U.K. His research interests include sparse representations, wireless networks, deep learning, and distributed systems.



IAN J. WASSELL received the B.Sc. and B.Eng. degrees from the University of Loughborough, Loughborough, U.K., in 1983, and the Ph.D. degree from the University of Southampton, Southampton, U.K., in 1990. He is a Senior Lecturer in the Computer Laboratory, University of Cambridge, Cambridge, U.K. He has in excess of 15 years experience in the simulation and design of radio communication systems gained via a number of positions in industry and higher education. He has published more than 180 papers concerning wireless communication systems. His research interests include fixed wireless access, sensor networks, cooperative networks, propagation modeling, compressive sensing, and cognitive radio. He is a member of the IET and a Chartered Engineer.